Effect of Organic Solvent on the Permeability and Stiffness of Polyelectrolyte Multilayer Microcapsules

ARTICLE *in* MACROMOLECULES · MAY 2005

Impact Factor: 5.8 · DOI: 10.1021/ma050493y

7 AUTHORS, INCLUDING:

Byoung-Suhk Kim
Chonbuk National University
86 PUBLICATIONS **1,222** CITATIONS

SEE PROFILE

Olga I Vinogradova
Russian Academy of Sciences
111 PUBLICATIONS **3,382** CITATIONS

SEE PROFILE

Effect of Organic Solvent on the Permeability and Stiffness of Polyelectrolyte Multilayer Microcapsules

Byoung-Suhk Kim, Olga V. Lebedeva, Kaloian Koynov, Haofei Gong, Gunnar Glasser, Ingo Lieberwith, and Olga I. Vinogradova*

Max Planck Institute for Polymer Research, Ackermannweg 10, Mainz 55128, Germany

Received March 8, 2005; Revised Manuscript Received April 18, 2005

ABSTRACT: The effect of postmodification of polyelectrolyte multilayer microcapsules by exposure to organic solvent/water mixtures on their permeability, morphology, and mechanical properties is investigated. We study microcapsules with ultrathin shells composed of alternating polystyrene sulfonate and polyallylamine hydrochloride. Ethanol and acetone are used as organic solvents. In pure water, the high-molecular-weight dextran cannot diffuse through the shells of microcapsules. However, the addition of even a small amount of ethanol or acetone allows its fast encapsulation. We demonstrate that a mechanism of encapsulation in ethanol and acetone solutions is fundamentally different. In case of ethanol/water mixtures, the reason for encapsulation is the contraction of coils of the encapsulated polymer. No changes in the shell morphology, its nanopore structure, or mechanical properties as compared with those in pure water were detected. In contrast, in the case of acetone/water mixtures, the encapsulation reflects the true permeability changes of the shells caused by a formation of large nanopores. This is accompanied by a significant softening of the capsules. Our results suggest that electrostatic screening caused by addition of organic solvent does not play any significant role in the control of permeability and mechanical properties of polyelectrolyte multilayer microcapsules.

1. Introduction

Polyelectrolyte multilayer microcapsules[1,2] represent new composite microstuctures of special interest. The nanoshell of these capsules is formed by a polyelectrolyte multilayer with well-defined structure and thickness.[3−5] It is commonly accepted that the electrostatic interaction between oppositely charged polyelectrolytes is the main driving force for the multilayer assembly as well as the main factor for its stability.[4,6] Among the factors controlling the structure of multilayers, the charge density of polyelectrolytes and ionic strength of a surrounding solution are reported to be of main importance.[7−9] The same factors were shown to be of primary importance in determining the microcapsule mechanics.[10] Thus, the variation of the multilayer shell stiffness with added salt[11−13] and pH[12,14] has been recently reported. There have also been some data indicating that pH and salt may influence the permeability of the multilayer shell.[15−17]

It is natural to suggest that another possibility to regulate thickness, porosity, and mechanical properties of multilayer shells is to use organic solvents. A posttreatment of capsules in organic solvents or their mixtures with water can modify the interaction between shell-forming polyelectrolytes. One reason is that organic solvents and their mixtures with water have much lower dielectric constants as compared with pure water, which should lead to the effective screening of electrostatic interaction within the multilayer. Besides that, organic solvents could affect the interaction between hydrophobic fragments present in some polyelectrolytes. Thus, it appears that organic solvent/water mixtures of various compositions can be used to tune the structure and mechanical properties of multilayer films forming the capsule shells.

The effect of organic solvent on the structure parameters and properties of polyelectrolyte multilayer microcapsules, and in fact even supported multilayers, has not received enough attention so far. Until now, there have been only a few studies of the influence of ethanol on the assembly of supported multilayers.[6,18] However, little is known about possible changes in thickness due to a posttreatment of multilayers by organic solvents. There have been some reports that the addition of ethanol or acetone to water can enhance the permeability of the multilayer shell for high-molecular-weight polymers. Thus, 50% ethanol/water mixtures were used to encapsulate urease,[19] and 50% acetone/water mixtures were used to encapsulate dextran[20] and polystyrene sulfonate.[21,22] However, despite successfully performed encapsulation, the mechanism of permeability changes remains unclear and was never addressed before. There have been suggestions that ethanol[19] and acetone[20] induce the reversible formation of relatively large nanopores in the capsule shells, but this hypothesis so far was never supported by any experimental data. To our knowledge, the question of possible influence of organic solvent on the mechanical properties of multilayer microcapsules was never addressed before. There have been some indirect indications that acetone might act as a shell plasticizer,[23] but no direct confirmation of this hypothesis was obtained so far.

The present work is a detailed investigation of the influence of organic solvent/water mixtures of various compositions on the mechanical properties and permeability of polyelectrolyte multilayer microcapsules. As before, we study capsules with shells composed of alternating poly(sodium 4-styrenesulfonate) (PSS) and poly(allylamine hydrochloride) (PAH). As a polymer for a permeability test, we use fluorescently labeled neutral-polymer FITC-dextran of a high molecular weight. As organic solvents, we use acetone and ethanol. Our choice of these two particular solvents is motivated by recent studies where their mixtures with water were employed to encapsulate macromolecules,[14,19,20] and by the fact that both solvents and their mixtures with water do

* Author to whom correspondence should be addressed. Email: vinograd@mpip-mainz.mpg.de.

10.1021/ma050493y CCC: $30.25
Published on Web 05/17/2005

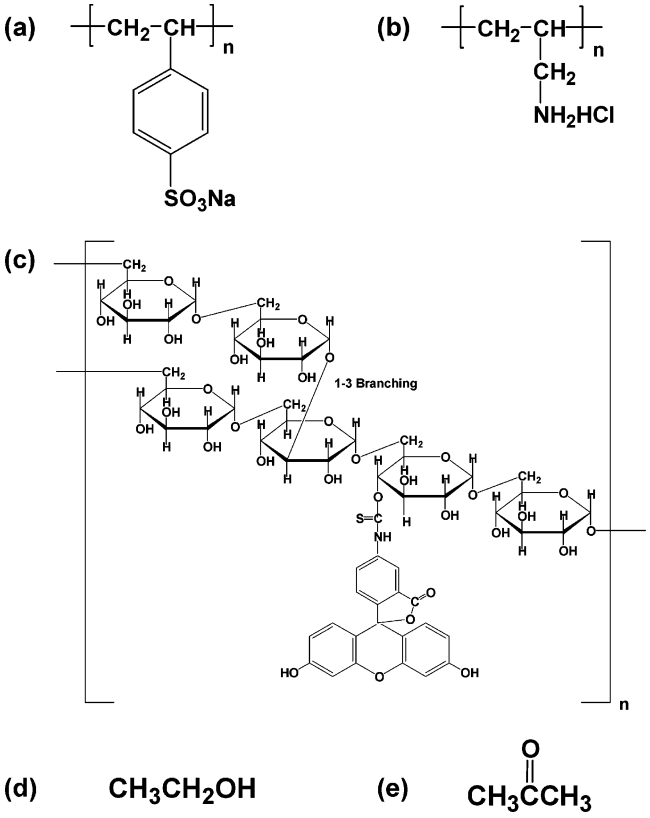

Figure 1. Chemical structures of PSS (a), PAH (b), FITC-dextran (c), ethanol (d), and acetone (e).

have very close values of dielectric constants.[24]

After describing the details of experimental measurements of multilayer film thickness, morphology of the shell, its permeability, and mechanical properties in the following section, we present results and discussion. Then follows a concluding section.

2. Experimental Section

2.1. Materials. The fluorescent dye fluorescein isothiocyanate (FITC), shell-forming polyelectrolytes poly(sodium 4-styrenesulfonate) (PSS; $M_w \sim 70$ kDa) and poly(allylamine hydrochloride) (PAH; $M_w \sim 70$ kDa) were purchased from Sigma-Aldrich Chemie GmbH, Germany. FITC-dextran ($M_w \sim 500$ kDa) were purchased from Aldrich and used as received. Sodium chloride (NaCl) was purchased from Riedel-de Haën, Germany. Acetone and ethanol were purchased from Fisher Scientific GmbH. All chemicals were of analytical purity or higher quality and were used without further purification. The chemical structures of PSS, PAH, FITC-dextran, ethanol, and acetone are shown in Figure 1.

Water used for all experiments was purified by a commercial Milli-Q Gradient A10 system containing ion-exchange and charcoal stages and had a high resistivity of 18.2 MΩ/cm.

The mixtures of acetone and ethanol with water with different concentrations of organic solvents were prepared. The parameters of mixtures used in experiments are summarized in Table 1.

Suspensions of monodisperse weakly cross-linked melamine formaldehyde particles (MF particles) with a radius of $r_0 = 2.0 \pm 0.1$ μm were purchased from Microparticles GmbH (Berlin, Germany). Glass bottom dishes (0.17 mm/∅ 30 mm) with optical-quality surfaces were obtained from World Precision Instruments Inc. (USA). Glass spheres (radius 20±1 μm) were purchased from Duke Sci. Co., California. The glass prism and LaSFN9 substrates for surface plasmon experiments were purchased from Hellma Optik, Germany.

2.2. Methods. Capsule Preparation. The positively charged MF particles (50 μL of 10 wt % dispersion) as a template were incubated with 1 mL of PSS solution (1 mg/mL containing 0.5 mol/L NaCl, pH 6) for 10 min, followed by three centrifugation/rinsing cycles, and finally dispersed in water. 1 mL of a PAH solution (1 mg/mL containing 0.5 mol/L NaCl, pH 6) was then added to the particle dispersion. After 10 min given for adsorption, three centrifugation/wash cycles were performed (as above). The PSS and PAH adsorption steps were repeated four times each to build multilayers on the MF particles. The microcapsules were obtained by dissolving the MF template in HCl at pH 1.2−1.6 and washing with water three times as described before.[25]

Table 1. Parameters of Mixtures Used in Experiments

vol %	dielectric constant[24]	viscosity,[38] 10^{-2} g/cm·s	refractive index[39,40]
	Ethanol		
0	78.5	1.003	1.333
25	66.8	2.180	1.347
50	53.5	2.862	1.359
75	39.1	2.315	1.365
100	24.3	1.204	1.361
	Acetone		
0	78.5	1.003	1.333
25	60.6	1.478	1.348
50	43.5	1.552	1.361
75	29.0	1.020	1.366
100	20.7	0.328	1.359

Surface Plasmon Resonance Spectroscopy (SPR). A home-built surface plasmon resonance spectrometer (SPR) was used for the thickness measurements of the multilayer films deposited on a planar surface. The sample was attached to the base of a glass prism optically matched by index oil. A beam of a He−Ne laser (632.8 nm) with transverse-magnetic polarization was directed through the prism. By rotating the prism, the angle of the incident beam relative to the surface was adjusted (Figure 2). Collection of the reflected light with a photodiode (PD) mounted on a second, collinear goniometer allowed for angle-resolved reflectivity measurements (see ref 26 for more details).

To prepare substrates for SPR measurements, we first thermally evaporated a gold layer with a thickness of 50 nm with high refractive index ($n = 1.8$) $LaSFN_9$ substrates. The gold film was then functionalized by a self-assembled monolayer of 3-mercaptopropionic acid (Aldrich) (3MPA) by immersing the substrates in a 0.03 mol/L solution of 3MPA for 3 h. Such a modified surface is negatively charged in water. Afterwords, these substrates were used for multilayer film build up, which was produced by layer-by-layer (LbL) self-assembly of four pairs of PSS and PAH. Both PSS and PAH solutions were of concentration 1 mg/mL and were assembled

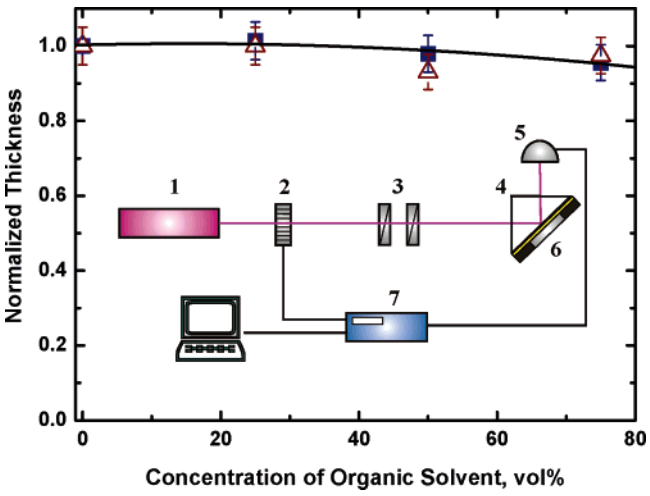

Figure 2. Ratio of thickness of PSS/PAH multilayers in water/ethanol (filled squares) and water/acetone (open triangles) solutions to that in pure water. Inset shows the schematic of SPR experiment: 1, laser; 2, chopper; 3, polarizers; 4, prism; 5, photodiode; 6, sample; 7, lock-in amplifier.

in the presence of 0.5 mol/L NaCl. Each adsorption step took 10 min and followed with a thorough rinsing with Milli-Q water (three times) to remove all excess of polymer and salt. The assembled multilayer films were then immersed into acetone or ethanol solutions for 24 h. The SPR measurements were carried out in a Teflon flow cell. This allowed us to measure the thickness of the multilayers immersed into mixtures of acetone and ethanol with water. The optical thickness of the samples was analyzed by a "Winspall" software on the basis of the transfer matrix evaluation method. The refractive index was assumed to be 1.5. This assumption was based on the previous work[27−29]

Confocal Laser Scanning Microscopy (CLSM). We used a commercial confocal microscope unit FV300 (Olympus, Japan) and an inverted fluorescence microscope Olympus IX70. To make confocal images of capsules, the high-resolution (60×) bright (NA = 1.45) immersion oil objective was used. The time of confocal scanning of the capsules was 1−2 s. The fluorescence intensity profiles were measured at the equatorial plane.

Capsule Deformation Experiment. The experimental setup for the force measurements was described before.[12,23,30] Briefly, load (force) vs deformation curves were measured with the molecular force probe device (MFP) 1D (Asylum Co., Santa Barbara, USA), which has a nanopositioning sensor. This sensor can correct piezoceramic hysteresis and creep of the AFM piezotranslator. For force measurement, we used V-shaped cantilevers (Micromash, Estonia, spring constants k = 3 N/m). The spring constant of the cantilever was estimated from the resonance-frequency calibration plot (Cantilevers catalog, Micromash, Estonia). Glass spheres were glued onto the apex of cantilevers with epoxy glue (UHU Plus, Germany). The capsule deformation experiment has been described before.[12,23,30] Here, we performed the measurements at a piezotranslator speed of 20 μm/s. The result of measurement represents the deflection Δ versus the position of the piezotranslator at a single approach. The load force F was determined from the cantilever deflection, $F = k\Delta$. As before, we assume that the zero of separation is at the point of the first measurable force.[12,23,30] Then the deformation is calculated as the difference between the position of the piezotranslator and cantilever deflection. The diameter of the capsule was determined optically with an accuracy of 0.2 μm and from the AFM load versus deformation curves (like in refs 12, 23, and 30). The size of the capsules was determined as an average of at least 10−15 capsules. The relative deformation ϵ of the capsule was then calculated as $\epsilon = 1 - H/(2r)$, where H is the minimum sphere/substrate separation,[23,30] and r is the capsule radius. To get reliable results, we have performed several series of force measurements. Every series included at least 10−15 experiments for each solution. Then the average of all force versus deformation curves for each organic solvent/water mixture was calculated.

Scanning Electron Microscopy (SEM). For scanning electron microscopy (SEM) analysis, a drop of each sample solution was applied to a silicon wafer with sequential drying at room temperature for 2−3 h. The measurements were performed using a Gemini LEO (Zeiss) 1530 instrument operating at a working distance of 2 mm and an acceleration voltage of 0.5 kV. Because the samples were not covered with a gold layer before inspection, this low-acceleration voltage was applied to avoid charging of the sample. The images were recorded using the InLens detector.

Transmission Electron Microscopy (TEM). For TEM examination, one drop of sample solution was applied to a carbon-coated copper TEM grid. Excess solution was blotted off with a piece of filter paper. The remaining sample solution on the carbon film was allowed to dry at room temperature before examination by TEM. Inspection of the dry capsules was performed in a LEO 912 transmission electron microscope at an acceleration voltage of 120 kV. Images were taken on a 1k Proscan CCD camera. To get the pore size distribution, we have analyzed images of several capsules. At least 200 pores were measured for every sample. The radius of pores was taken as an average of size corresponding to several (at least six) cross-sections. Error of the measurements was estimated to be 10%. Then the area of pores was estimated as the sum of area of all pores in the studied segment of a capsule. The relative area coated by pore was calculated as a ratio of an area coated by pores to the total area.

Atomic Force Microscopy (AFM). The AFM images of dried capsules deposited on silicon wafers were taken in a tapping mode (Nanoscope IIIa, Digital Instruments). The silicon wafers were washed with *piranha solutions*, i.e., submerging the slides under a 3:1 (vol %) mixture of sulfuric acid and 30% hydrogen peroxide for at least 20 min at 80 °C to remove organic residues from substrates. At least three microcapsules in each sample were imaged. The images were analyzed with Nanoscope 5.30r1 software.

Fluorescence Correlation Spectroscopy (FCS). We used a commercial FCS setup manufactured by Carl Zeiss (Jena, Germany) consisting of the module ConfoCor 2 and an inverted microscope model Axiovert 200. For our experiments, we employed a Zeiss C-Apochromat 40x/1.2 W corr water immersion objective. The fluorophores were excited by an argon ion laser at 488 nm, and emissions were collected in a range between 530 and 600 nm. For detection, an avalanche photodiode enabling single-photon counting was used. The FITC-dextran solutions were freshly prepared and investigated immediately. The eight-well, polystyrene-chambered cover glass (Lab-Tek, Nalge Nunc International) and homemade glass chambers were used as sample cells for the water/ethanol and water/acetone solutions, respectively. Both types of cells had bottom slides with optical quality surfaces and a thickness of 0.17 mm. For each solution, a series of 20 measurements with a total duration of 5 min were performed. The autocorrelation function was analyzed by fitting the data with the commercial software supplied with the microscope (see Appendix for the details).

Dynamic Light Scattering (DLS). For the dynamic light scattering (DLS) experiment, we used a commercial instrument (ALV-5000 GmbH/Langen, Germany). An ALV-5000E correlator was used to measure the correlation function of scattered light. The measurements were carried out in the angular range $30° < \theta < 150°$ at room temperature. A Kr-ion laser was used as the light source (wavelength $\lambda = 647.1$ nm). A cylindrical cell having an inner diameter of 18 mm was placed in a thermostated bath. All solutions were filtered directly into the cylindrical cell through a 0.45 μm membrane filter (Millipore).

3. Results and Discussion

3.1. Thickness of the Multilayers. To investigate the response of the multilayers to ethanol/water and acetone/water mixtures, a supported PSS/PAH four-bilayer film was assembled from aqueous solutions containing 0.5 mol/L NaCl, and its thickness in salt-free ethanol/water and acetone/water mixtures was determined. Measurements were performed after 24 h of contact with the corresponding mixture. The results are presented in Figure 2. The changes in the film thickness were found to be the same for both solvents. At relatively small concentrations of organic solvents, we have not detected any changes in the optical thickness of the multilayers. A small (less than 5%) decrease in the multilayer thickness was observed only at high (50−75%) concentrations of organic solvent. We have previously studied the influence of salt postmodification on the thickness of the same PSS/PAH multilayers.[13] A swelling of the multilayers at low ionic strength and a significant decrease in the film thickness at high ionic strength have been observed. The swelling was attributed to a breaking of the numbers of ionic cross-links in the "tethered" state of the multilayer. The decrease in thickness was shown to be caused by dissociation/deconstruction of the multilayer, or its "melted" state.[13] Our results here clearly suggest that

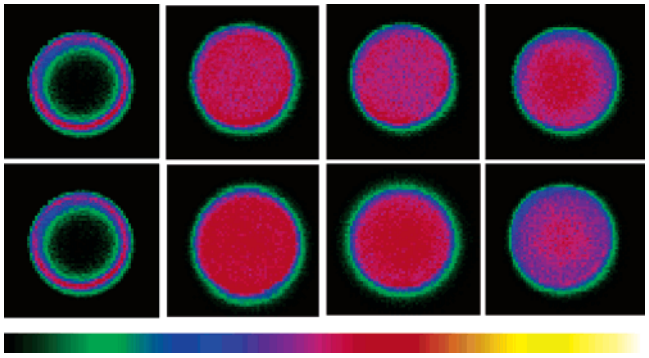

Figure 3. Confocal images of capsules immersed into a solution of 500 kDa FITC-dextran. The top is the case of acetone and the bottom ethanol. From left to right the concentrations of organic solvent: ~0, 25, 50, and 75%. Color bar indicates the mapping of intensity of fluorescence value to color: from left to right the intensity changes from 0 to 1 au.

the effect of an organic solvent is different from the effect of an increase in ionic strength. Both breaking of physical (ionic or hydrophobic, caused by possible interaction of styrene groups) cross-links or desorption of polyelectrolytes should be ruled out according to our SPR data. To our knowledge, there has been a recent attempt to explore if the postdeposition exposure of multilayer films prepared from standard aqueous electrolyte solutions containing NaCl ethanol/water mixtures influences the multilayer thickness.[18] A dramatic decrease in the film thickness was found at about 40% of ethanol. Most likely, this difference from our observation results is due to a combined effect of salt and ethanol. The change in thickness of our multilayers, treated by salt-free acetone/water and ethanol/water solutions, should be considered as negligibly small. We should, therefore, rule out any possibility of influence of the change in the film thickness caused by organic solvents on the permeability and mechanical properties of capsules presented below.

3.2. Permeability Test. To explore the influence of type and concentration of organic solvent on diffusion permeability of multilayer shells, we have studied quantitatively the possibility of encapsulating a high-molecular-weight polymer, FITC-dextran, from different water/organic solvent mixtures. The multilayer microcapsules were exposed to FITC-dextran solutions (2×10^{-7} mol/L) containing different amounts of ethanol and acetone for 30 min. After this, dispersions of microcapsules were thoroughly rinsed with water, and the distribution of the intensity of fluorescence inside the capsules was measured. The typical confocal images of the microcapsules are shown in Figure 3. The interior of the capsules exposed in pure water remains dark, suggesting that the multilayer shell is not permeable for FITC-dextran. This observation is consistent with earlier reports.[10,15,19−21,31] However, the interior of the capsules exposed in organic solvent/water mixtures containing FITC-dextran is fluorescent, which indicates the encapsulation of fluorescently labeled molecules. The brightness of the capsule interior does not change with time, and there was no fluorescent signal from water. This proves that the multilayer shells are again in an impermeable state. To quantify the encapsulation, we have measured the fluorescence intensity distribution across the capsules. The averaged profiles of fluorescence intensities coming from the capsule interiors are presented in Figure 4. We note that encapsulated FITC-dextran is uniformly distributed inside microcapsules. In our previous experiments with the encapsulated polyelectrolytes, we always observed the enhanced fluorescence intensity from the shells caused by polyelectrolyte adsorption.[14,21,22] Essentially, there is no difference in the amount of FITC-dextran encapsulated from 25% and 50% ethanol/water and acetone/water mixtures. Moreover, for 25% mixtures, the intensity of fluorescence inside capsules was found to be roughly equal to that (2×10^{-7} mol/L) corresponding to a bulk solution of FITC-dextran used for encapsulation. Therefore, a small amount of added acetone or ethanol allows perfect encapsulation of FITC-dextran so that it is not necessary to use much more concentrated mixtures or a larger encapsulation time as before.[19−21] We have, however, found that there is a small difference in the degree of encapsulation from 75% mixtures. In the case of an acetone/water mixture, we have reached the same complete encapsulation as for less concentrated solutions. The concentration of FITC-dextran encapsulated using 75% ethanol/water mixture was found to be often 10−15% smaller than in the initial bulk solution.

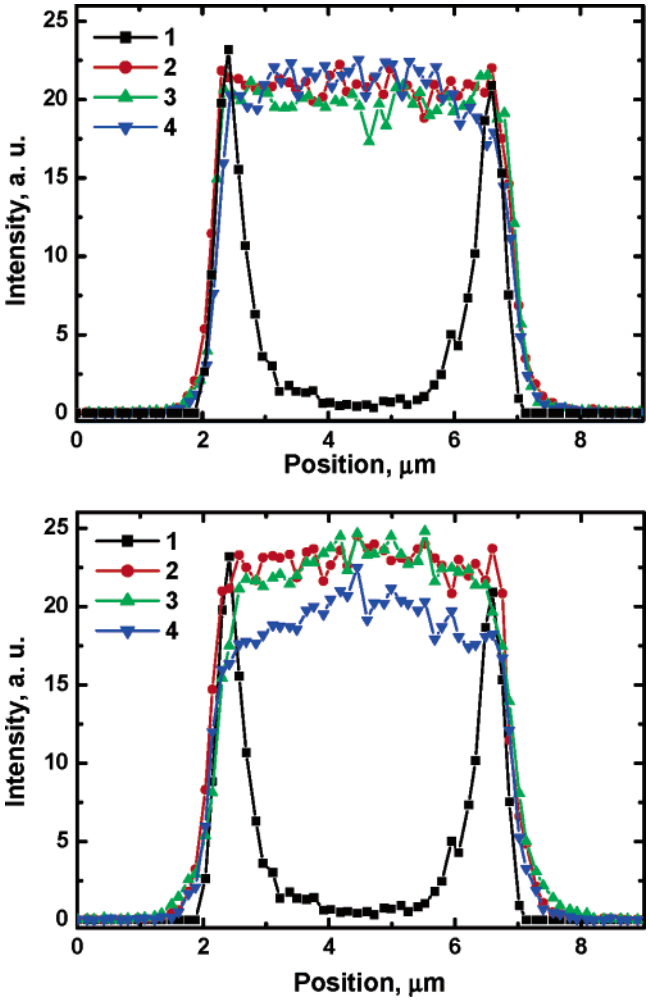

Figure 4. Average distribution of fluorescence intensity across the capsules immersed in a solution of dextran in water (1) and organic solvent/water mixtures: 25 (2), 50 (3), and 75% (4) of organic solvent. Top, acetone; bottom, ethanol.

3.3. Force-Deformation Profiles. Figure 5 and Figure 6 show typical force vs relative deformation profiles for capsules measured in water, ethanol/water, and acetone/water mixtures. Measurements were performed after 24 h of a contact with the corresponding

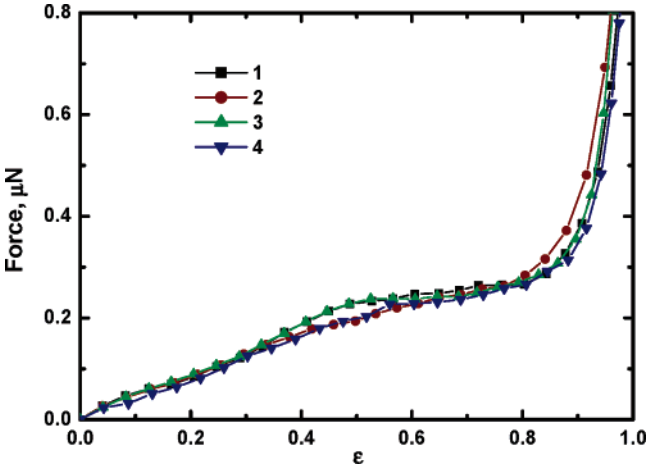

Figure 5. Force-deformation curves measured in water (1) and ethanol/water mixtures 25 (2), 50 (3), and 75% (4). Only every 15th point is shown.

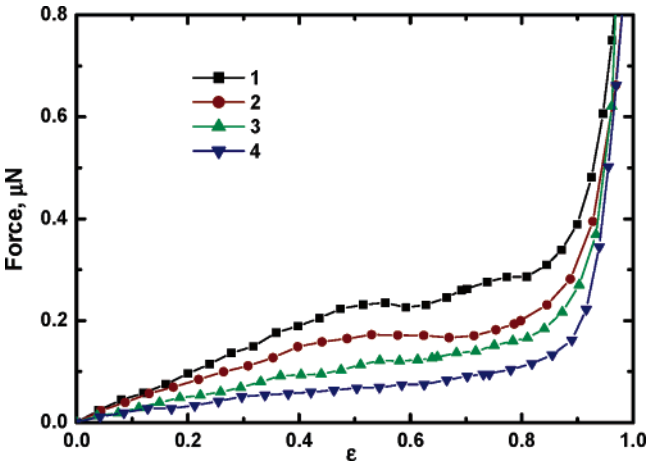

Figure 6. Force-deformation curves measured in water (1) and acetone/water mixtures 25 (2), 50 (3), and 75% (4). Only every 15th point is shown.

mixture. The stiffness of capsules was found to be largest in water. It remains the same in all ethanol/water mixtures, indicating that ethanol does not influence mechanical properties of the capsules. On the contrary, the stiffness of capsules measured in acetone/water mixtures decreased with the concentration of acetone. These results are in remarkable contrast with the SPR and permeability data described above, where no significant difference between the effect of two solvents was found.

3.4. SEM. To explore the multilayer shell morphology more closely, we have taken and analyzed SEM images of dried capsules. Figure 7 shows SEM images of dried capsules after their immersion in water, ethanol/water, and acetone/water mixtures. All collapse upon drying by forming structures with folds and creases.[20,23,30] The surface morphology of microcapsules treated by ethanol was found to be identical to what was observed for microcapsules initially immersed in water. The microcapsules treated by an acetone/water mixture show a different morphology with folds with much smoother edges. This indicates some plastification of multilayers. The observation is consistent with the effect of softening in acetone/water mixtures because the plastification of the shell should result in a smaller Young's modulus.

3.5. TEM and AFM Analysis of a Nanopore Structure. Because the softening of capsules and their

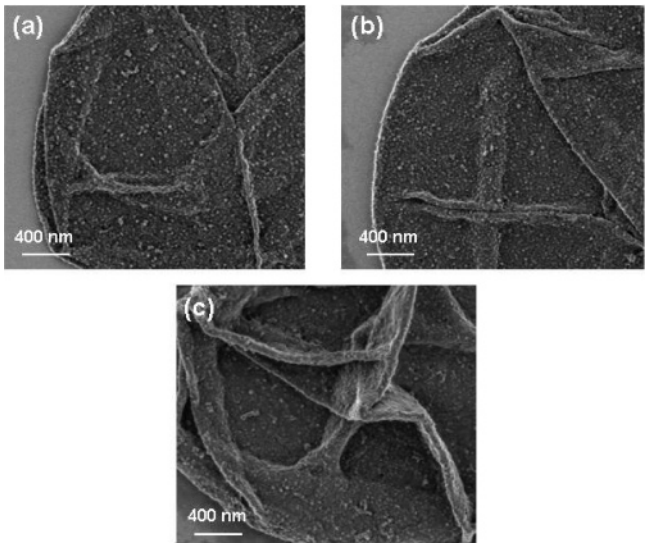

Figure 7. SEM images of capsules initially immersed in water (a), 50% water/ethanol mixtures (b), and 50% water/acetone mixture (c).

permeability could be connected with the formation of nanopores, we have also addressed the issue of nanopore structure of the multilayer.[32] Previously, high-resolution SEM was used to detect both small nanopores[32] and larger, pH-induced, pores.[33] However, here we found that the direct comparison of detected with SEM nanopore structure of samples is impossible because of complications caused by significant roughening of acetone-treated capsules. Therefore, we decided to use both TEM and AFM imaging for this purpose. The AFM imaging was used before to prove the existence of large, pH-induced, nanopores in the shells.[34] To the best of our knowledge, the TEM analysis was never performed before to explore the nanopore structure of the shells.

Figure 8 shows TEM bright-field micrographs of dried capsules after their immersion in water, ethanol/water, and acetone/water mixtures. In comparison with SEM, TEM additionally provides a more detailed view on the morphology of the multilayer of the capsules. Because the dried capsules consist only of PSS and PAH, which should give similar contrast in TEM observation, the bright areas reflect a decrease in local thickness. Hence, they can be interpreted as holes in the capsule shell or simply as pores.

The total area covered by the pores is estimated to be ~1% for the capsules immersed in water, 1% and 4% for the capsules immersed in ethanol/water and acetone/water mixtures, respectively. The analysis of the pore size distribution in water shows that the absolute majority of them have a radius of 5−10 nm. We have not found any significant changes in the pore size for capsules posttreated by ethanol/water mixtures. For the capsules treated in acetone/water mixtures, we, however, see the distinct change in pore size distribution. The relative amount of small pores of a radius below 10 nm decreases by a factor of 2. This is accompanied by the appearance of large pores with a highly irregular, noncircular shape. An averaging of linear sizes measured in several directions suggests that the mean radius of a large pore is above 40 nm.

The TEM data were confirmed by AFM imaging (Figure 9). For microcapsules initially immersed in water, no nanopores were detected. This indicates that nanopores, if any, are smaller than the radius of the

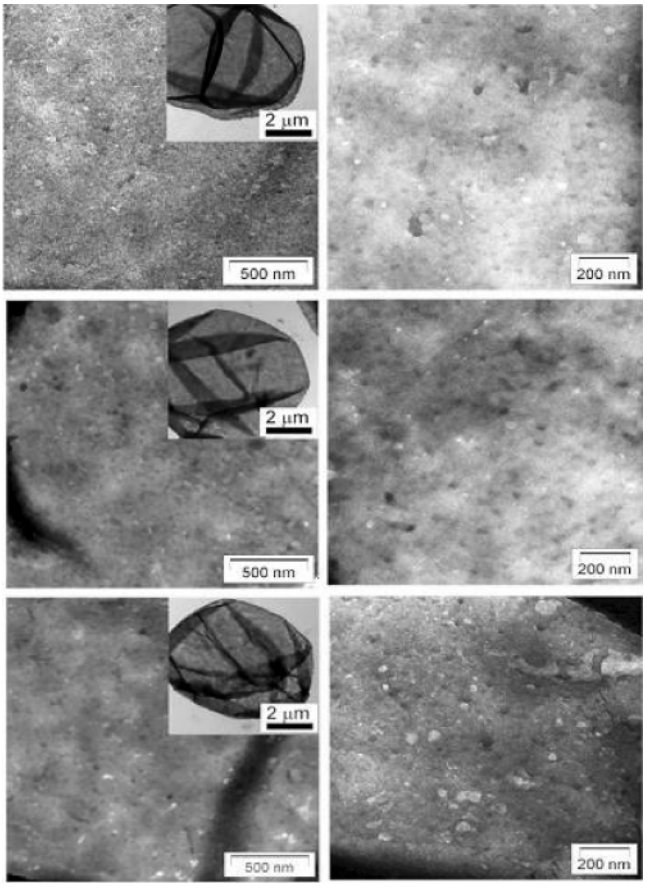

Figure 8. TEM images of capsules initially deposited in water (top), 50% water/ethanol mixtures (middle), and 50% water/acetone mixture (bottom).

AFM tip (~10 nm). The AFM images of microcapsules treated by ethanol/water mixtures show similar morphology. In contrast, capsules treated by acetone/water solutions show highly porous morphology. The linear size of the pores is ranged from 30 to 100 nm. The depth of the pores is about 20 nm, which indicates that they are the real holes in the multilayer.

3.6. FCS Measurements of the Radius of an Encapsulated Polymer. In the context of no changes in morphology and nanopore structures of the multilayer shells treated in ethanol/water solutions, the natural assumption would be that the observed apparent changes in the permeability of the shells are due to conformation changes of FITC-dextran molecules. We, therefore, have measured the hydrodynamic radius of FITC-dextran.

Because FITC-dextran molecules carry highly fluorescent chromophores, fluorescence correlation spectroscopy (FCS) is a straightforward method to study the size of the molecules and their aggregation properties.[35−37] We have evaluated the hydrodynamic radius (R_H) of FITC-dextran in acetone/water and ethanol/water solutions using the procedure described in the Appendix. The results are shown in Figure 10. In pure water, the hydrodynamic radius of FITC-dextran was found to be 13.1 nm. This is in reasonable agreement with the value of 15.7 nm, which we have extrapolated from the dependence of R_H vs M_w provided from Aldrich for FITC-dextran of M_w below 150 kDa. This value exceeds the nanopore size. That is probably why no encapsulation was possible in pure water.

As can be seen from Figure 10, in ethanol/water solutions, R_H initially decreases with the ethanol concentration, reaching a minimal value of 8.5 nm at about 25% ethanol and then increases again up to 12.6 nm at 75% mixture. An initial decrease in R_H is likely due to the fact that the solvent is becoming poorer. As a result, the contraction of FITC-dextran coils begins. An increase in R_H at a higher concentration of ethanol indicates that some aggregation starts. Most likely, in a 75% ethanol mixture, we deal with dimers of single contracted coils of a radius of ~6.3 nm. These observations are crucial. They confirm that the apparent changes in permeability of multilayer shells in ethanol/water mixtures are not connected with the change in the shell properties and reflect only the conformational

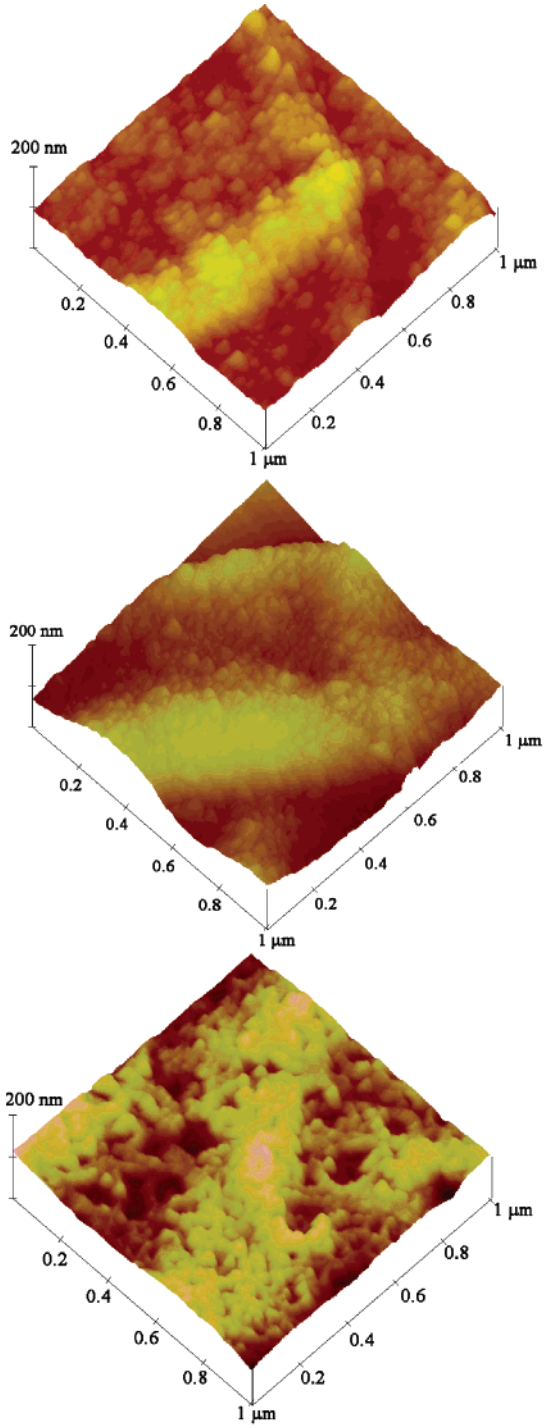

Figure 9. AFM images of capsules after deposition in water (top), 50% water/ethanol mixtures (middle), and 50% water/acetone mixture (bottom).

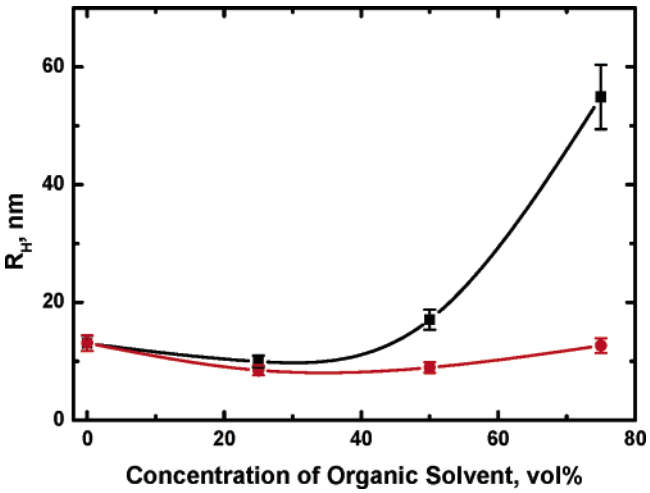

Figure 10. Hydrodynamic radius of FITC-dextran in water/acetone (squares) and water/ethanol (circles) solutions as measured by FCS.

changes of encapsulated polymers. Indeed, perfect encapsulation was observed in 25% and 50% of ethanol/water mixtures, i.e., in the situation when no aggregation was detected and the radius of FITC-dextran coils was smaller than the size of nanopores. The encapsulation was less successful in 75% solutions where the radius of FITC-dextran aggregates was comparable with the radius of nanopores.

For acetone/water solutions, the trend is similar. In this case, however, a strong aggregation of FITC-dextran molecules was observed for the 75% acetone/water mixture, leading to an average value of $R_H \sim 55$ nm. Such value apparently corresponds to aggregates of several dextran molecules. This, however, does not affect the degree of encapsulation because the large acetone-induced pores are formed and allow diffusion of even large aggregates through the multilayer shell.

It is important to stress here that very diluted solutions with a FITC-dextran concentration of about 0.5 μg/mL ($\sim 10^{-9}$ mol/L) were used for FCS experiments. This concentration is lower than that used for encapsulation. For comparison, we have used dynamic light scattering to measure the hydrodynamic radius of FITC-dextran at the organic solvent/water mixtures, but with higher concentration of the dextran molecules, typically about 0.2 mg/mL ($\sim 4 \times 10^{-7}$ mol/L). This is a minimal concentration possible in DLS experiments, which is, however, higher than that used for encapsulations. The DLS experiments have shown a dependence of the hydrodynamic radius on the concentration of the organic solvent that is qualitatively the same as those measured by FCS and plotted in Figure 10. The absolute values of R_H evaluated from DLS, however, were slightly larger than those measured with FCS. This is most likely related to the formation of aggregates even in pure aqueous solutions because of the higher concentration of FITC-dextran used for the DLS experiments.

4. Concluding Remarks

Several aspects of our work warrant further comments.

First, we have found that the permeability, morphology, and mechanical properties of multilayer microcapsules do not depend on the dielectric constant of a solvent. We studied mixtures of two organic solvents, ethanol and acetone, with water. Essentially, the mixtures of the same composition have roughly the same dielectric constants for both solvents (Table 1). However, the effect of these solvents on the morphology of the shells and their mechanical properties differs dramatically. Whether this conclusion is valid in general or only for highly nonideal mixtures (see Table 1) used in this work remains an open question. The fact, however, remains: we have not found any correlation between the values of dielectric constants of the solvent and the multilayer shell properties.

Second, the successful encapsulation does not necessarily mean the change in permeability of the multilayer shell as it was suggested before.[19,34] Here, we show that there exists an alternative way of encapsulation connected with the contraction of polymer coils caused by organic solvent. This phenomenon takes place in low-concentration solutions of organic solvents and is entirely responsible for encapsulation from ethanol/water mixtures.

Third, we have proven that some solvents (acetone in this paper) can lead to dramatic changes in shell permeability through the reversible formation of large pores in the multilayers. Similar pores were induced before by varying the pH of solutions.[33,34] The phenomenon of large pore formation is poorly understood at the moment and has to be studied in more detail.

In summary, we have presented data describing the effect of ethanol and acetone on the permeability and mechanical properties of polyelectrolyte multilayer microcapsules. Our results show that the effect of ethanol on the PSS/PAH multilayer capsules is no effect. No changes in the thickness of the shells, their morphology, or nanopore structures, as well as in mechanical properties, were detected. The apparent changes in the shell permeability for a high-molecular-weight polymer were proven to reflect nothing more than a contraction of polymer coils in ethanol/water mixtures. The effect of acetone on the PSS/PAH multilayer shells is that of softening. The observed softening correlates with the significant changes in morphology of the shells and the formation of large pores. These pores are responsible for an enhanced permeability of the multilayer shells for high-molecular-weight polymers.

Acknowledgment. B.S.K. and H.G. acknowledge the financial support of the Alexander von Humboldt Foundation. We thank F. Gröhn, C. Holm, A. R. Khokhlov, V. Lobaskin, H. Schiessel, M. R. Stukan, and G. B. Sukhorukov for helpful discussions. We are also grateful to A. Best, K. Vasilev, and R.Kita for experimental advice, and B. Müller for light scattering measurements.

Appendix: Determination of the Hydrodynamic Radius of FITC-Dextran Molecules with FCS

The fluorescence correlation spectroscopy (FCS) technique is an important tool for investigation of the dynamic properties of single molecules in solution. The method is based on detecting and analyzing the fluorescence from chromophores diffusing through a small and fixed volume element V, usually formed by a laser focus of submicron waist size. From the measured fluctuations of the fluorescence intensity $I(t)$, an autocorrelation function

$$G(t) = \frac{\langle I(t' + t)I(t')\rangle}{\langle I(t')\rangle} \quad (1)$$

corresponding to the probability of a particle inside the volume V at time t' to be still inside after a time t can be determined.

It can be shown that, for an ensemble of different fractions of ideal particles with Brownian diffusive motion and a Gaussian profile of the volume element V, the autocorrelation function has the form:

$$G(t) = \frac{1 + \frac{Tr}{1 - Tr} e^{-t/\tau_{Tr}}}{N} \left(\sum_{i=M}^{M} \frac{F_i}{(1 + t/\tau_i)\sqrt{1 + t/(S^2\tau_i)}} \right) + 1 \quad (2)$$

where M is the number of fluorescent components, N is the average number of fluorescent molecules in the detection volume, Tr and τ_{Tr} are, respectively, the fractional population and decay time of the triplet state, F_i and τ_i are, respectively, the contribution and translational diffusion time of the ith fluorescent component, and S is the "structural" parameter of the instrumental setup: $S = z_0/\omega_0$, where z_0 and ω_0 are the distances from the center of the laser beam focus in the axial and radial directions, respectively, at which the collected fluorescence intensity has dropped by a factor of e^2 compared to its peak value for the Gaussian beam profile. A numerical fit of the experimentally determined autocorrelation curve (1) with the theoretical function (2) can yield important parameters of the system i.e., F_i, τ_i, N, and S.

For fluorescent particles with a hydrodynamic radius R_H much smaller than the detection volume ($R_H < \omega_0$), the diffusion coefficient D can be determined from the diffusion time τ, as $D = \omega_0^2/4\tau$. Finally the hydrodynamic radius of the particles can be calculated using the Stokes−Einstein equation:

$$R_H = \frac{k_B T}{6\pi\eta D} \quad (3)$$

where T is the temperature, k_B the Boltzmann constant, and η the viscosity of the solution.

With this in mind, we have used the following procedure for determination of the hydrodynamic radius of FITC-dextran molecules in acetone/water and ethanol/water mixtures. First, we measured the autocorrelation function of diluted ($\sim 10^{-8}$ mol/L) aqueous solution of rhodamine 6G, which is commonly considered as a calibration standard with known diffusion coefficient $D = 2.8 \times 10^{-10} m^2 s^{-1}$. This function was fitted with eq 2 using the fitting software of our FCS module ConfoCor 2 (Carl Zeiss, Jena, Germany), and the diffusion time for rhodamine 6G as well as the focal radius ω_0 and the structure parameter S of our setup were determined. With these parameters known and fixed, we have measured and fitted the autocorrelation curves of water/acetone and water/ethanol solutions of FITC-dextran to determine the corresponding diffusion coefficients D.

It is important to emphasize at this point that, if the sample solutions (acetone/water and ethanol/water mixtures) have refractive indices different than those of the immersion medium of the objective (pure water), some aberration may appear and therefore the focal radius ω_0 and the structure parameter S may change. As can be seen from Table 1, however, even the most concentrated (75%) acetone/water and ethanol/water mixtures exhibit refractive indices only slightly higher than those of pure water. For that reason, we have neglected any aberration effects and kept ω_0 and S fixed.

Finally, from the diffusion coefficients D, using the Stokes−Einstein eq 3 and corresponding values of the viscosity (shown in Table 1), we have calculated the hydrodynamic radius R_H of the FITC-dextran molecules in the different acetone/water and ethanol/water mixtures.

References and Notes

(1) Donath, E.; Sukhorukov, G. B.; Caruso, F.; Davis, S.; Möhwald, H. *Angew. Chem., Int. Ed.* **1998**, *37*, 2202−2205.
(2) Sukhorukov, G. B.; Donath, E.; Lichtenfeld, H.; Knippel, E.; Budde, A.; Mohwald, H. *Colloids Surf., A* **1998**, *137*, 253−266.
(3) Decher, G. *Science* **1997**, *277*, 1232−1237.
(4) Bertrand, P.; Jonas, A.; Laschewsky, A.; Legras, R. *Macromol. Rapid Commun.* **2000**, *21*, 319−348.
(5) Hammond, P. T. *Adv. Mater.* **2004**, *16*, 1271−1293.
(6) Dubas, S. T.; Schlenoff, J. B. *Macromolecules* **1999**, *32*, 8153−8160.
(7) Dubas, S. T.; Schlenoff, J. B. *Langmuir* **2001**, *17*, 7725−7727.
(8) McAloney, R. A.; Dudnik, V.; Goh, M. C. *Langmuir* **2003**, *19*, 3947−3952.
(9) Sukhishvili, S. A.; Granick, S. *J. Am. Chem. Soc.* **2000**, *122*, 9550.
(10) Vinogradova, O. I. *J. Phys.: Condens. Matter* **2004**, *16*, R1105−R1134.
(11) Vinogradova, O. I.; Lebedeva, O. V.; Vasilev, K.; Gong, H.; Garcia-Turiel, J.; Kim, B. S. *Biomacromolecules* **2005**, *6*, 1495−1502.
(12) Lulevich, V. V.; Vinogradova, O. I. *Langmuir* **2004**, *20*, 2874−2878.
(13) Lebedeva, O. V.; Kim, B. S.; Vasilev, K.; Vinogradova, O. I. *J. Colloid Interface Sci.* **2005**, *284*, 455−462.
(14) Kim, B. S.; Vinogradova, O. I. *J. Phys. Chem. B* **2004**, *108*, 8161−8165.
(15) Sukhorukov, G. B.; Antipov, A. A.; Voigt, A.; Donath, E.; Möhwald, H. *Macromol. Rapid Commun.* **2001**, *22*, 44−46.
(16) Antipov, A. A.; Sukhorukov, G. B.; Möhwald, H. *Langmuir* **2003**, *19*, 2444−2448.
(17) Ibarz, G.; Dähne, L.; Donath, E.; Möhwald, H. *Adv. Mater.* **2001**, *13*, 1324−1327.
(18) Poptoshev, E.; Schoeler, B.; Caruso, F. *Langmuir* **2004**, *20*, 829−834.
(19) Lvov, Y.; Antipov, A. A.; Mamedov, A.; Möhwald, H.; Sukhorukov, G. B. *Nano Lett.* **2001**, *1*, 125−128.
(20) Lulevich, V. V.; Radtchenko, I. L.; Sukhorukov, G. B.; Vinogradova, O. I. *Macromolecules* **2003**, *36*, 2832−2837.
(21) Vinogradova, O. I.; Andrienko, D.; Lulevich, V. V.; Nordschild, S.; Sukhorukov, G. B. *Macromolecules* **2004**, *37*, 1113−1117.
(22) Lebedeva, O. V.; Kim, B. S.; Vinogradova, O. I. *Langmuir* **2004**, *20*, 10685−10690.
(23) Lulevich, V. V.; Andrienko, D.; Vinogradova, O. I. *J. Chem. Phys.* **2004**, *120*, 3822−3826.
(24) Akerlöf, G. *J. Am. Chem. Soc.* **1932**, *54*, 4125−41239.
(25) Sukhorukov, G. B.; Donath, E.; Davis, S.; Lichtenfeld, H.; Caruso, F.; Popov, V. I.; Möhwald, H. *Polym. Adv. Technol.* **1998**, *9*, 759−767.
(26) Knoll, W. *Annu. Rev. Phys. Chem.* **1998**, *49*, 569−638.
(27) Vasilev, K.; Knoll, W.; Kreiter, M. *J. Chem. Phys.* **2004**, *120*, 3439−3445.
(28) Picart, C.; Sengupta, K.; Schilling, J.; Maurstad, G.; Ladam, G.; Bausch, A. R.; Sackmann, E. *J. Phys. Chem. B* **2004**, *108*, 7196−7205.
(29) Ruths, J.; Essler, F.; Decher, G.; Riegler, H. *Langmuir* **2000**, *16*, 8871.
(30) Lulevich, V. V.; Radtchenko, I. L.; Sukhorukov, G. B.; Vinogradova, O. I. *J. Phys. Chem. B* **2003**, *107*, 2735−2740.
(31) Antipov, A. A.; Sukhorukov, G. B.; Leporatti, S.; Radtchenko, I. L.; Donath, E.; Mohwald, H. *Colloids Surf., A* **2002**, *198*, 535−541.
(32) Lulevich, V. V.; Nordschild, S.; Vinogradova, O. I. *Macromolecules* **2004**, *37*, 7736−7741.
(33) Mendelsohn, J. D.; Barrett, C. J.; Chan, V. V.; Pal, A. J.; Mayes, A. M.; Rubner, M. F. *Langmuir* **2000**, *16*, 5017−5023.
(34) Antipov, A. A.; Sukhorukov, G. B. *Adv. Colloid Interface Sci.* **2004**, *111*, 49−61.
(35) Elson, E. L.; Magde, D. *Biopolymers* **1974**, *13*, 1−27.

(36) Magde, D.; Elson, E. L.; Webb, W. W. *Biopolymers* **1974**, *13*, 29−61.
(37) Minard-Basquin, C.; Weil, T.; Hohner, A.; Rädler, J. O.; Müllen, K. *J. Am. Chem. Soc.* **2003**, *125*, 5832−5838.
(38) Dizechi, M.; Marschall, E. *J. Chem. Eng. Data* **1982**, *27*, 358−363.
(39) David, R. L. *CRC Handbook of Chemistry and Physics*, 66th ed.; CRC Press: Boca Raton, 1985−1986.
(40) Kurtz, S. S.; Wikingsson, A. E.; Camin, D. L.; Thompson, A. R. *J. Chem. Eng. Data* **1965**, *10*, 330−334.

MA050493Y